

An Optimal Observable Machine for reinterpretable measurements in high-energy physics

Torben Mohr ,^{a,b} Alejandro Quiroga Triviño ,^a Fabian Riemer ,^a Artur Monsch ,^a Matteo Defranchis ,^c Joscha Knolle ,^a Ankita Mehta ,^c Jan Kieseler ,^a and Markus Klute ^a

^a Karlsruhe Institute of Technology (KIT), Karlsruhe, Germany

^b Ghent University, Ghent, Belgium

^c European Organization for Nuclear Research (CERN), Geneva, Switzerland

E-mail: torben.mohr@cern.ch, alejandro.quiroga.trivino@cern.ch,
fabian.riemer@student.kit.edu, artur.artemij.monsch@cern.ch,
matteo.defranchis@cern.ch, joscha.knolle@cern.ch,
ankita.mehta@cern.ch, jan.kieseler@cern.ch, markus.klute@cern.ch

ABSTRACT: A machine-learning-based framework for constructing generator-level observables optimized for parameter extraction in particle physics analyses is introduced, referred to as the Optimal Observable Machine (OOM). Unfoldable differential distributions are learned that maximize sensitivity to a parameter of interest while remaining robust against detector effects, systematic uncertainties, and biases introduced by the unfolding procedure. Detector response and systematic uncertainties are explicitly incorporated into the training through a likelihood-based loss function, enabling a direct optimization of the expected measurement precision while minimizing the bias from any assumption on the parameter of interest itself. The approach is demonstrated in an application to top quark physics, focusing on the measurement of a recently observed pseudoscalar excess at the top quark pair production threshold in dilepton final states. It is shown that a generator-level observable with enhanced sensitivity and long-term reinterpretablility can be constructed using this method.

Contents

1	Introduction	1
2	Observable finding	2
3	Optimal observable for toponium	5
3.1	Simulated event samples	5
3.2	Training setup	6
3.3	Results from detector-level training	7
3.4	Results from generator- and detector-level training	7
4	Conclusions	10

1 Introduction

Extracting physical parameters from experimental data is a central task in particle physics. This includes precision measurements of standard model (SM) parameters and searches for new physics, which are often interpreted as constraints on beyond-the-SM models. In both cases, parameters are inferred by comparing the measured distributions of carefully chosen observables with theoretical predictions, taking into account both the sensitivity of the observable and the achievable experimental precision.

Traditionally, observables are constructed based on physical intuition or analytical considerations and unfolded to the parton or particle level (i.e., defined purely in terms of parton or particle information before detector reconstruction, also referred to as “generator level”), enabling direct comparison with theoretical predictions. Alternatively, templates can be generated at the level of reconstructed objects using detector simulation (“detector-level”), often offering higher sensitivity [1]. However, performing the detector simulation is computationally expensive and at high precision generally only feasible within experimental collaborations [2–4]. As a result, reinterpretations by the broader community typically rely on unfolded measurements, e.g., Refs. [5, 6] for recent examples.

The increasing use of machine-learning methods has made detector-level analyses more powerful, but also more complex [7]. While such approaches have enabled increasingly precise parameter extractions, their complexity often prevents straightforward reinterpretation, limiting the long-term usability, or “shelf life”, of the resulting measurements.

In this work, we introduce the *Optimal Observable Machine* (OOM), a machine-learning-based framework for constructing unfoldable observables that are optimally suited for parameter extraction. Rather than selecting observables *a priori*, the OOM *learns* an unfoldable differential distribution that is explicitly tailored to a given parameter of interest.

The learned observable is designed to maximize sensitivity to the parameter while remaining robust against detector effects, systematic uncertainties, and biases introduced by the unfolding procedure. As a result, the OOM yields unfolded generator-level measurements that combine high precision with long-term reinterpretablity.

Top quark physics plays a central role in the study of fundamental interactions. As the heaviest known elementary particle, the top quark is a sensitive probe of important SM parameters, such as the top quark mass, as well as of potential new physics at higher energy scales [8]. To illustrate the capabilities of the OOM, we apply it to a recent example of top quark analyses performed by the ATLAS and CMS Collaborations. Using proton-proton collision data recorded at $\sqrt{s} = 13$ TeV, the experiments reported the observation of a pseudoscalar excess at the top quark pair ($t\bar{t}$) production threshold [9–11], which can be interpreted as a “toponium” bound state and/or attributed to a new pseudoscalar boson [12–20]. We employ the OOM to obtain a generator-level observable with optimal sensitivity to distinguish between the pseudoscalar excess and the continuum $t\bar{t}$ production contribution.

The use of machine-learning methods to construct optimal detector-level observables is a well-established technique in measurements and searches of the ATLAS and CMS experiments [21–31]. Recent machine-learning developments have incorporated systematic uncertainties in the observable optimization [32–37]. We build the OOM on top of the approach from Ref. [37], which we extend to the optimization of generator-level observables.

2 Observable finding

The goal of the OOM is to find an observable \mathcal{O} with a generator-level differential cross section $d\sigma/d\mathcal{O}$ that simultaneously fulfills the following goals:

- (i) It is defined exclusively through generator-level information.
- (ii) It maximizes sensitivity to the parameter of interest c .
- (iii) It is precisely measurable in the presence of systematic uncertainties.
- (iv) It has minimal dependence on theoretical uncertainties and model assumptions.

The corresponding detector-level distribution is denoted by $x_{\mathcal{O}}$, such that $d\sigma/d\mathcal{O}$ can be measured by applying unfolding to $x_{\mathcal{O}}$ [38]. In an idealized scenario without background contributions, the response matrix R encodes all detector and reconstruction effects relevant for the unfolding, such that the following relation holds:

$$x_{\mathcal{O}}(c, \omega) = R(c, \omega) \frac{d\sigma}{d\mathcal{O}}(c, \omega). \quad (2.1)$$

Here, $d\sigma/d\mathcal{O}$ and $x_{\mathcal{O}}$ are to be understood as vectors with entries representing the bins of the two distributions. Generally, all three quantities $d\sigma/d\mathcal{O}$, $x_{\mathcal{O}}$, and R depend on c , as well as on nuisance parameters representing the effect of various sources of systematic uncertainties, denoted collectively by ω . The number of generator- and detector-level bins is not required to be the same, and thus R is not necessarily square.

Instead of constructing the observable by hand, we determine $d\sigma/d\mathcal{O}$ through a learnable deterministic function Φ_g as:

$$\frac{d\sigma}{d\mathcal{O}}(c, \omega) = \mathcal{H}[\Phi_g(f_g(c, \omega))], \quad (2.2)$$

where \mathcal{H} denotes the histogramming (or binning) operation and f_g represents a set of generator-level features. These features have to be selected such that they provide sensitivity to c , which is how the sensitivity of $d\sigma/d\mathcal{O}$ to c is achieved. However, the features generally also depend on the systematic uncertainties ω , and thus cause a dependence of $d\sigma/d\mathcal{O}$ on ω . Through this construction, goal (i) is automatically fulfilled, and any reinterpretation of a measurement of $d\sigma/d\mathcal{O}$ can be performed without requiring detector simulation. Similarly, we determine $x_{\mathcal{O}}$ as:

$$x_{\mathcal{O}}(c, \omega) = \mathcal{H}[\Phi_d(f_d(c, \omega))], \quad (2.3)$$

depending on a set f_d of detector-level features, with similar considerations for the dependence on c and ω as for f_g . In practice, Φ_g and Φ_d are implemented as multilayer perceptrons (MLPs) and trained simultaneously.

To achieve goal (ii), we consider a loss function for the MLP training that rewards a precise extraction of c from the optimized observable. Starting from the binned likelihood function \mathcal{L} that represents the measurement of c , we calculate the Hessian matrix

$$H_{\alpha\beta} = \frac{\partial^2}{\partial\alpha\partial\beta}(-\log\mathcal{L}), \quad (2.4)$$

where the derivatives are taken with respect to c and the nuisance parameters, i.e., $\alpha, \beta \in \{c, \omega\}$. We can then calculate the expected uncertainty in c , denoted by Δc , from the diagonal element of the inverted Hessian matrix:

$$\Delta c = \sqrt{H_{cc}^{-1}}, \quad (2.5)$$

which is used directly as the loss function during the training. This approach, described in more detail in Ref. [37], utilizes the Fisher information formalism [39] for the case of the Asimov data set [40], i.e., when considering the expected sensitivity.

The likelihood function for a binned profile likelihood fit with nuisance parameters is formulated as:

$$\mathcal{L} = \mathcal{L}_p(d | x_{\mathcal{O}}(c, \omega)) \cdot \mathcal{L}_{\text{NP}}(\omega), \quad (2.6)$$

where \mathcal{L}_p represents the Poisson likelihood to obtain the observed data distribution, denoted by d , given the prediction $x_{\mathcal{O}}(c, \omega)$, and \mathcal{L}_{NP} encompasses penalty terms for all nuisance parameters ω [41, 42]. Incorporating systematic uncertainties through \mathcal{L}_{NP} in the loss function is a central aspect of the *systematic-uncertainty-aware training* as introduced in Ref. [37], ensuring that the training goal aligns with the final precision of the measurement of c even in cases where systematic uncertainties become comparable to or dominant over statistical uncertainties.

Training Φ_d with a loss function based on Eq. (2.6) would yield a detector-level distribution with maximal sensitivity to c that is precisely measurable in the presence of systematic uncertainties. We extend this approach to an *unfolding-aware training* by substituting $x_{\mathcal{O}}$ via Eq. (2.1) in the likelihood function:

$$\mathcal{L} = \mathcal{L}_p \left(d \left| R(c, \omega) \frac{d\sigma}{d\mathcal{O}}(c, \omega) \right. \right) \cdot \mathcal{L}_{\text{NP}}(\omega), \quad (2.7)$$

This way, we phrase the training as a search for the generator-level distribution $d\sigma/d\mathcal{O}$ that has maximum sensitivity to c (ii) in the presence of systematic uncertainties (iii), including those that affect the generator-level distribution (iv). Since R is determined from the definitions of $d\sigma/d\mathcal{O}$ and $x_{\mathcal{O}}$, the resulting loss function is sensitive to the definition of $x_{\mathcal{O}}$ as well.

A critical aspect of the method is to ensure gradient flow through all learnable parameters. We aim for a single-utility optimization based on Eq. (2.7). At each gradient descent step, Φ_g and Φ_d are evaluated and the response matrix is determined from their binned output. We then calculate:

$$\tilde{x}_{\mathcal{O}}(c, \omega) = \frac{1}{2} \left\{ R(c, \omega) \mathcal{H}[\Phi_g(f_g(c, \omega))] + \mathcal{H}[\Phi_d(f_d(c, \omega))] \right\}, \quad (2.8)$$

and evaluate

$$\mathcal{L} = \mathcal{L}_p(d \left| \tilde{x}_{\mathcal{O}}(c, \omega) \right.) \cdot \mathcal{L}_{\text{NP}}(\omega). \quad (2.9)$$

While the result is identical compared to the usage of Eq. (2.7) directly with respect to the forward evaluation, this procedure introduces explicit gradients into both Φ_g and Φ_d from the training on detector level.

A technical aspect that requires special care in this context is the treatment of histogram binning. Since the loss function is defined in terms of binned distributions, gradients must be propagated through the binning operation in order to enable end-to-end training. This necessitates a differentiable formulation of the binning step, which assigns events to bins in a smooth manner while preserving the interpretation of the resulting histograms as approximate counts. We use the approach proposed in Ref. [37] for the one-dimensional distributions as well as for the two-dimensional response matrix.

In any unfolding approach, prior assumptions on c have to be made in order to calculate R . Since R generally carries a dependence on c , this can lead to a bias in the unfolded distribution. With c_0 being the nominal hypothesis and c_{α} representing a set of alternative values, we can evaluate the folded distributions $x_{\mathcal{O},\alpha} = R(c_{\alpha}) d\sigma/d\mathcal{O}(c_0)$, i.e., folding the nominal generator-level distribution with the different hypotheses for the response matrices, and quantify the bias by calculating the difference between $x_{\mathcal{O},\alpha}$ and the nominal result $x_{\mathcal{O},0}$. To minimize the dependence of R on c and ensure a good reinterpretability of the unfolded we result, we add the following penalty term to the loss function used in the OOM:

$$\lambda \exp \sum_{\alpha} \chi^2(x_{\mathcal{O},\alpha}, x_{\mathcal{O},0}), \quad (2.10)$$

where λ is a parameter that governs the strength of the constraint. This way, the training favors observables for which R is approximately independent of c , meaning that the sensitivity on $x_{\mathcal{O}}$ on c must predominantly originate from $d\sigma/d\mathcal{O}$ through Eq. (2.1).

Finally, background contributions can be incorporated in a straightforward manner. Backgrounds that are independent of c are added at the detector level to $x_{\mathcal{O}}$, including their dependence on ω . If a background contribution itself depends on c , it may instead be treated as part of the signal, either by incorporating it into the learned generator-level distribution or by modeling it through an additional response matrix. It is also possible to introduce regularization into the unfolding procedure if desired in the usual way by adding additional penalty terms [38].

3 Optimal observable for toponium

We apply the OOM to the measurement of toponium in dilepton final states. In Refs. [9–11], the ATLAS and CMS Collaborations construct three-dimensional distributions at detector level using:

- the reconstructed invariant mass of the top quark pair, denoted by $m_{t\bar{t}}$;
- the scalar product of the unit vectors of the momenta of the two leptons in the rest frames of their parent top quark and antiquark, respectively, denoted by c_{hel} ;
- a similar scalar product but with the sign of the component parallel to the top quark direction flipped for one of the leptons, denoted by c_{han} .

The spin correlation variables c_{hel} and c_{han} provide sensitivity to distinguish between a scalar or pseudoscalar contribution of the observed excess, whereas $m_{t\bar{t}}$ provides sensitivity to the mass of the excess. We consider the signal strength r of the toponium sample, i.e., the ratio of the measured cross section to the prediction, as the parameter of interest (i.e., c in the notation of Section 2), and demonstrate how to find an optimal observable both at generator- and detector-level to constrain r in the presence of systematic uncertainties.

3.1 Simulated event samples

The OOM is applied using simulated event samples including a fast detector simulation. We employ `MADGRAPH5_aMC@NLO` 2.6.5 [43] for the matrix-element calculation, the `NNPDF3.1NLO` [44] parton distribution functions, `PYTHIA` 8.310 [45] for the simulation of parton shower, fragmentation, and hadronization, and `DELPHES` 3.5.0 [46–48] with its default CMS detector configuration for the detector response and pileup effects. The considered scenario is the Run 3 data-taking period of the LHC, i.e., we simulate proton-proton collisions at $\sqrt{s} = 13.6$ TeV and assume an integrated luminosity of 300 fb^{-1} for the normalization of the event counts.

Samples for $t\bar{t}$ production at next-to-leading order in perturbative quantum chromodynamics (simply referred to as “ $t\bar{t}$ sample” in the following) and for the production of a pseudoscalar resonance η_t in the final state $\eta_t \rightarrow W^+ b W^- \bar{b}$ (“ η_t sample”) are generated. A value of 172.5 GeV is used for the top quark mass. Top quark decays in the $t\bar{t}$ samples are simulated with `MADSPIN` [49], and the sample is normalized to a predicted cross section of $924^{+32}_{-40} \text{ pb}$, as calculated with `TOP++` 2.0 [50]. The η_t sample uses a simplified model for a generic resonance [14, 51] with mass set to 343 GeV (twice the top quark mass minus a

binding energy of about 2 GeV [51]) and width to 2.8 GeV (twice the top quark width [52]), following the setup in Ref. [9]. It is normalized to a cross section of 7.1 fb, obtained from scaling the predicted 13 TeV cross section of 6.4 fb [9, 51, 53] with the ratio of the $t\bar{t}$ cross sections at 13.6 and 13 TeV [50].

At the generator level, a fiducial selection is applied requiring exactly two electrons and/or muons with opposite charge and at least two jets, of which at least one is matched to a b quark. Similarly, an event selection is applied at the detector level. In both selections, electrons are required to have transverse momentum $p_T > 25$ GeV and pseudorapidity $|\eta| < 2.5$, muons to have $p_T > 25$ GeV and $|\eta| < 2.4$, and jets to have $p_T > 30$ GeV, $|\eta| < 2.5$, and an angular separation $\Delta R = \sqrt{(\Delta\eta)^2 + (\Delta\phi)^2} > 0.4$ from any selected lepton, where $\Delta\eta$ and $\Delta\phi$ are the differences in η and azimuthal angle, respectively. To emulate an efficient lepton identification, we additionally require detector-level electrons and muons to be geometrically matched to a selected generator-level lepton.

3.2 Training setup

We train two MLPs Φ_g and Φ_d , implemented in PYTORCH [54] with three hidden layers with 100 nodes each and a ReLU activation function [55] after each layer. The output layer uses a sigmoid activation function. Following Ref. [37], we first perform a pretraining of each MLP to optimize the separation between fiducial η_t and fiducial $t\bar{t}$ events. We then perform the simultaneous training as outlined in Section 2, using fiducial events from both samples as signal contributions and nonfiducial events as background contributions. The parameter of interest is the toponium signal strength r , which is only applied to the fiducial η_t events, so we can rewrite Eq. (2.1) as:

$$x_{\mathcal{O}}^{t\bar{t}}(\omega) + x_{\mathcal{O}}^{\eta_t}(r, \omega) = R(r, \omega) \left[\frac{d\sigma^{t\bar{t}}}{d\mathcal{O}}(\omega) + \frac{d\sigma^{\eta_t}}{d\mathcal{O}}(r, \omega) \right], \quad (3.1)$$

with a common response matrix R for both processes that can generally depend on r .

The generator-level features f_g are p_T and η of the top quark and antiquark; $\Delta\eta$, $\Delta\phi$, and ΔR between the top quark and antiquark; and $m_{t\bar{t}}$, c_{hel} , and c_{han} evaluated with generator-level objects. At the detector level, the reconstruction of the four-momenta of the top quark and antiquark is nontrivial. We apply a full kinematic reconstruction (FKR) [56], which reconstructs the top quark and antiquark four momenta by imposing constraints on the W boson and top quark mass and finding algebraic solutions for the neutrino momenta, as well as a loose kinematic reconstruction (LKR) [57], which reconstructs $m_{t\bar{t}}$ only and not the individual momenta, but does not require assumptions about the top quark mass. Since the FKR has a limited efficiency, i.e., it fails to provide a result for a relevant fraction of the events, we also use features that do not rely on top quark reconstruction. The detector-level features f_d used in the training are then:

- (without relying on top quark reconstruction) p_T and η of the two selected leptons and the up to four highest- p_T jets; $\Delta\eta$, $\Delta\phi$, and ΔR between the two leptons; ΔR between the two highest- p_T jets; the invariant mass of all selected leptons and jets; the scalar

sum of the p_T of all selected jets and leptons (H_T); the transverse sphericity [58] of the event;

- (using FKR) p_T and η of the top quark and antiquark; $\Delta\phi$ and ΔR between top quark and antiquark; $m_{t\bar{t}}$, c_{hel} , and c_{han} ;
- (using LKR) $m_{t\bar{t}}$.

We consider a limited set of systematic uncertainties, which are taken from the list of leading uncertainty sources in the CMS analysis [9]. As theoretical uncertainties, we include variations of the value of the strong coupling constant in the ISR and FSR simulation. As experimental uncertainty, we include a variation of the jet energy scale with magnitude similar to those in the ATLAS and CMS experimental analyses [59, 60]. Finally, we consider normalization uncertainties of 1% in the integrated luminosity and of 4% in the $t\bar{t}$ cross section.

3.3 Results from detector-level training

We first consider only the training of Φ_d to obtain an optimal observable for the measurement of r at the detector level. As a baseline scenario, we train Φ_d with only three input variables $m_{t\bar{t}}$, c_{hel} , and c_{han} (evaluated using FKR), i.e., using the variables used by the original analyses [9–11], and using cross-entropy (CE) [61] as loss function, which optimizes for the separation between $t\bar{t}$ and η_t production considering statistical uncertainties only. The first extended training considers the 29 input features listed above but still with CE as loss function. For the second extension, we apply the systematic-uncertainty-aware training [37]: the loss function is defined using a likelihood function corresponding to Eq. (2.6) that includes systematic uncertainty sources and is evaluated using the prediction of $x_{\mathcal{O}}$ under the nominal hypothesis for r as data d , i.e., using the Asimov data set [40]. Results of the three training strategies are compared in Fig. 1.

The negative log-likelihood scans (Fig. 1 left) show the precision in r achieved in the different scenarios. Using more event information significantly improves the sensitivity. It can also be seen that the analysis, in any scenario, is limited by systematic uncertainties. Using the systematic-uncertainty-aware training clearly improves the overall precision, even if the statistical uncertainty slightly increases. The difference between the CE and systematic-uncertainty-aware training also become visible in the feature importance ranking (Fig. 1 right): while the CE training relies the strongest on $m_{t\bar{t}}$ evaluated using LKR, the systematic-uncertainty-aware training instead relies more heavily on the ΔR between the two leptons and the highest lepton p_T , which are much less affected by the jet energy scale systematic uncertainty.

3.4 Results from generator- and detector-level training

Now we apply the full OOM with simultaneous optimization of both generator- and detector-level distributions. The likelihood function in Eq. (2.9) is used to define the loss function. Without the additional response-matrix constraint from Eq. (2.10), the MLPs

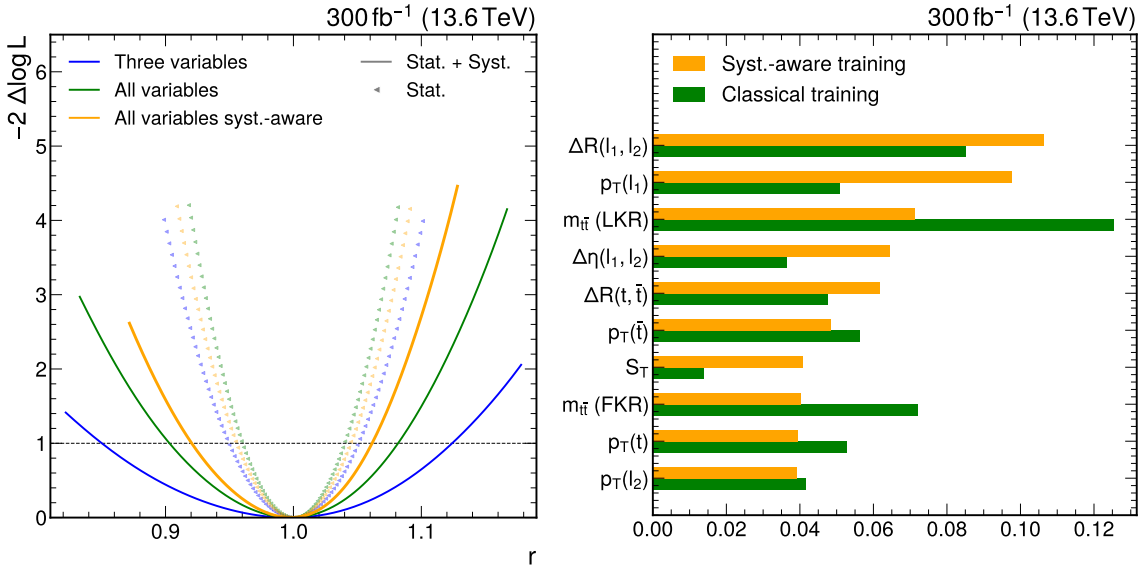


Figure 1. Results of different detector-level MLP training strategies. Left: Negative log-likelihood scans for the toponium signal strength r using CE training with three input variables (blue), CE training with 29 input variables (green), and systematic-uncertainty-aware training with 29 input variables (yellow). Shown are the scans using only statistical uncertainties (triangles) and using both statistical and systematic uncertainties (lines). Right: Feature importance ranking, evaluated using Ref. [62], for the ten most important input features, compared between the CE training (green) and the systematic-uncertainty-aware training (yellow), both using 29 input variables.

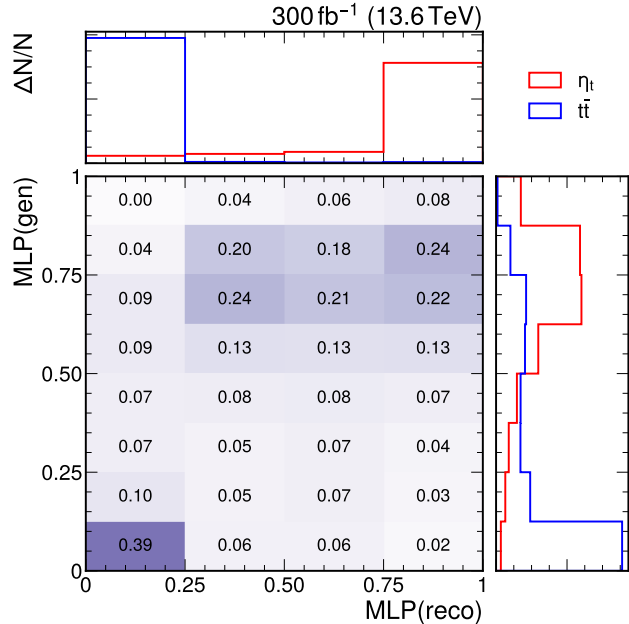


Figure 2. Response matrix R (main panel, with generator level on the x axis and detector level on the y axis), normalized distribution of $d\sigma/d\mathcal{O}$ at generator level (upper panel), and normalized distribution of $x_{\mathcal{O}}$ at detector level (right panel) for the OOM training without response-matrix constraint.

learn distributions such that both $x_{\mathcal{O}}$ and the folded distribution $R d\sigma/d\mathcal{O}$ are maximally sensitive to r . The result of this training is shown in Fig. 2.

To evaluate a possible bias from a direct dependence of R on r , we compare the detector-level distribution $x_{\mathcal{O}}$ with the folded distribution $R d\sigma/d\mathcal{O}$, separately for each of the two processes. The result of this comparison is shown in Fig. 3, providing also the Kolmogorov–Smirnov distance D_{KS} that quantifies the agreement between the two compared distributions. While the bias is small for $t\bar{t}$ production, which is the dominant contribution to R , we find a significant bias for η_t production. Since the total yield of selected $t\bar{t}$ events is more than 100 times larger than that of selected η_t events, it is clear that the response matrix is mainly derived from the $t\bar{t}$ events, which explains the bias found for the η_t sample.

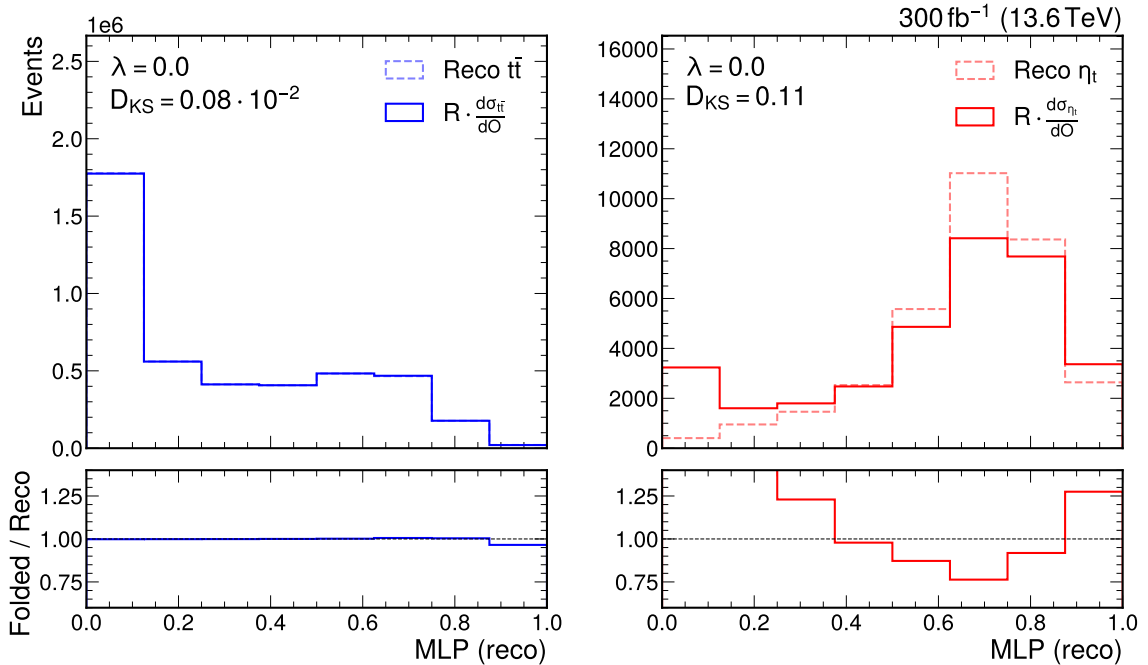


Figure 3. Comparison of the $t\bar{t}$ (left, blue) and η_t (right, red) yields between $x_{\mathcal{O}}$ (dashed) and the folded distribution $R d\sigma/d\mathcal{O}$ (solid). The lower panel displays the ratio between the two distributions. Shown are the results for the training without response-matrix constraint, i.e., with $\lambda = 0$. The captions list the Kolmogorov–Smirnov distance values.

To reduce this bias, we include the response-matrix constraint from Eq. (2.10) in the definition of the loss function. The strength λ of the constraint is then a hyperparameter of the training, and values $\lambda > 0$ reduce the bias. The comparison of the detector-level distributions for the example of a training with $\lambda = 0.25$ is shown in Fig. 4, showing a significantly reduced bias for the η_t production distribution.

We perform the training systematically for a range of possible λ values. For each value of λ , the training is performed 50 times to average out the randomness due to the initialization of the MLPs. To identify an optimal choice of λ , we evaluate both the bias via the value of D_{KS} and the overall precision in r obtained by evaluating Eq. (2.5) assuming the likelihood in Eq. (2.7). Figure 5 displays the D_{KS} results (left) and the expected precision

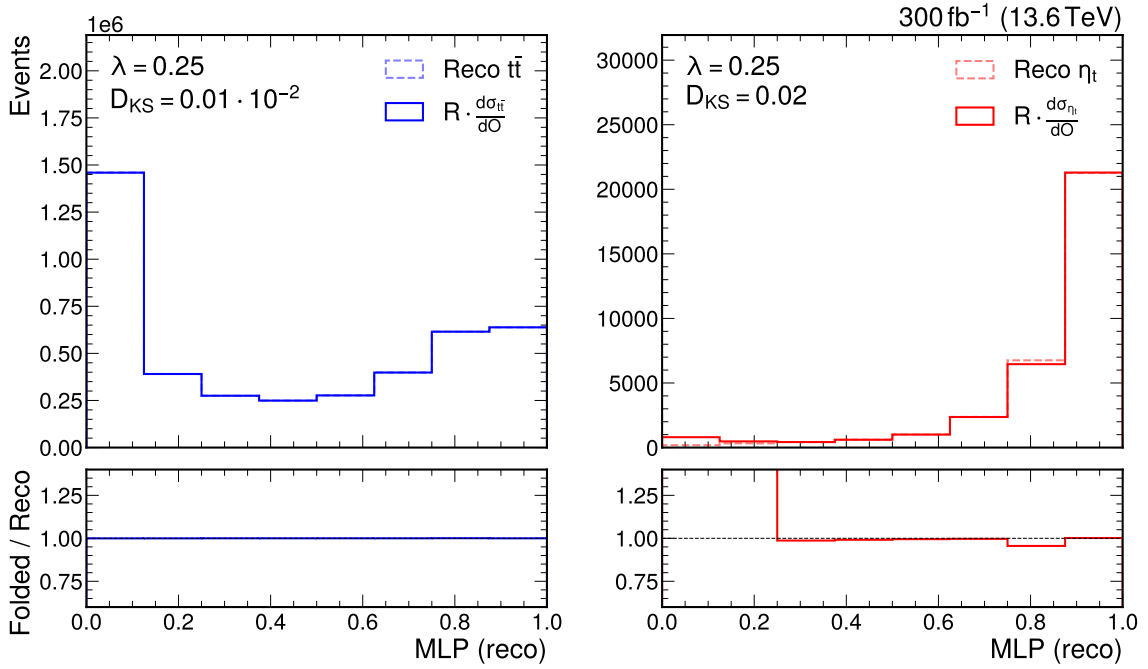


Figure 4. Comparison of the $t\bar{t}$ (left, blue) and η_t (right, red) yields between x_O (dashed) and the folded distribution $R d\sigma/dx_O$ (solid). The lower panel displays the ratio between the two distributions. Shown are the results for the training using the response-matrix constraint with $\lambda = 0.25$. The captions list the Kolmogorov–Smirnov distance values.

(right).

For $\lambda = 0$, the values of Δr are comparable with the results obtained by the systematic-uncertainty-aware training indicated by the red dotted line. While the introduction of the response-matrix constraint clearly reduces the bias and thus makes the unfolding less dependent on the parameter of interest r , this comes at the expense of sensitivity. For this application, a value of $\lambda = 0.25$ provides a good balance between high precision and low bias.

4 Conclusions

We present the *Optimal Observable Machine* (OOM), a machine-learning-based framework for the construction of generator-level observables optimized for parameter extraction. The key feature of the OOM is the explicit inclusion of detector response and systematic uncertainties in a likelihood-based training procedure, allowing the learned observable to be optimized directly for the expected measurement precision while remaining suitable for unfolding and reinterpretation.

The method combines detector-level and generator-level learnable functions and enforces consistency between them through the response matrix. To control biases arising from a parameter-dependent response, we introduce an explicit constraint that suppresses such dependencies. This enables the construction of observables whose sensitivity to the pa-

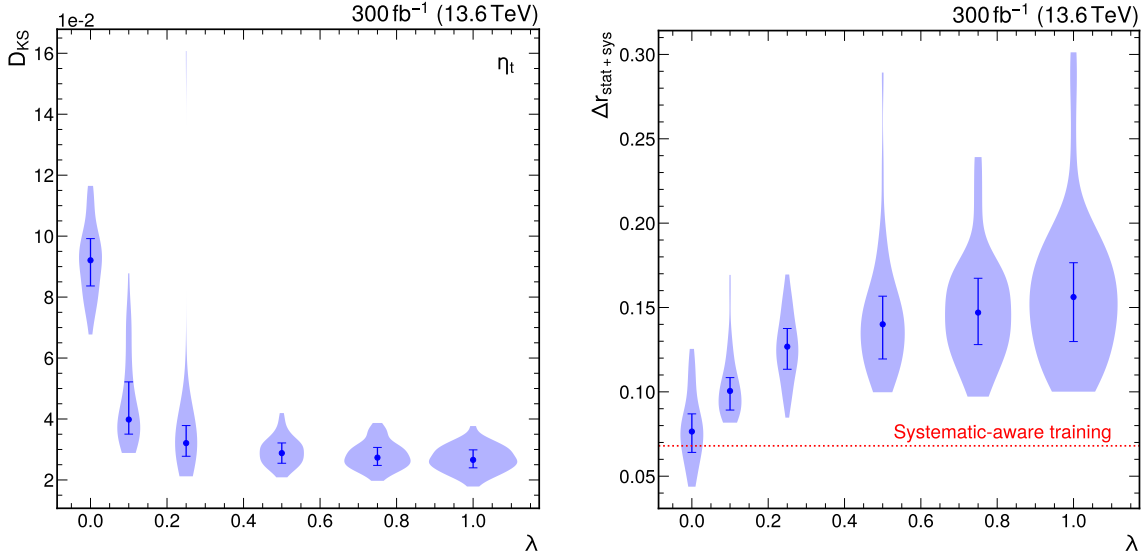


Figure 5. Results for different values of the response-matrix constraint strength λ . The violin plots show the distribution of the 50 trainings per λ value, the dots the median value, and the error bars the 25 and 75% quantiles. Left: Kolmogorov–Smirnov distance for the agreement between $x_{\mathcal{O}}$ and the folded distribution $R d\sigma/d\mathcal{O}$ shown for the η_t (right) yields. Right: Uncertainty in the η_t signal strength. The dotted red line indicates the uncertainty as obtained by the systematic-uncertainty-aware training shown in Fig. 1.

parameter of interest predominantly originates from the generator-level distribution, thereby preserving the conceptual advantages of unfolded measurements.

As a proof of principle, we apply the OOM to the measurement of a pseudoscalar excess at the top quark pair production threshold in dilepton final states. We demonstrate that the method yields a generator-level observable with enhanced sensitivity compared to traditional approaches, while maintaining a controlled dependence of the unfolding on the signal strength. The trade-off between bias and precision introduced by the response-matrix constraint was studied quantitatively, and an optimal working point was identified.

The OOM provides a general strategy for reconciling the high precision achievable with modern machine-learning techniques with the long-term interpretability of experimental results. As a next step, symbolic regression [63–65] can be applied to the learned generator-level distribution to obtain an analytic formulation of the observable, thus facilitating reinterpretations of the unfolded results without need for the implementation of the machine-learning models. While illustrated here in the context of top-quark physics, the method is broadly applicable to precision measurements and new-physics searches where unfolded observables are desired.

Acknowledgments

The authors thank the CERN summer student program, within which part of this work was carried out. In particular, T.M. and F.R. acknowledge the opportunity to be summer

students at CERN. Ja.K. was supported by the Alexander-von-Humboldt foundation during the initial phase of the project.

References

- [1] CMS Collaboration, “Review of top quark mass measurements in CMS”, *Phys. Rept.* **1115** (2025) 116, [doi:10.1016/j.physrep.2024.12.002](https://doi.org/10.1016/j.physrep.2024.12.002), [arXiv:2403.01313](https://arxiv.org/abs/2403.01313).
- [2] GEANT4 Collaboration, “GEANT4—a simulation toolkit”, *Nucl. Instrum. Meth. A* **506** (2003) 250, [doi:10.1016/S0168-9002\(03\)01368-8](https://doi.org/10.1016/S0168-9002(03)01368-8).
- [3] ATLAS Collaboration, “The ATLAS simulation infrastructure”, *Eur. Phys. J. C* **70** (2010) 823, [doi:10.1140/epjc/s10052-010-1429-9](https://doi.org/10.1140/epjc/s10052-010-1429-9), [arXiv:1005.4568](https://arxiv.org/abs/1005.4568).
- [4] CMS Offline Software and Computing Group, “CMS Phase 2 computing model: update document”, CMS Note CMS-NOTE-2022-008, 2022.
- [5] E. Celada et al., “Mapping the SMEFT at high-energy colliders: from LEP and the (HL)-LHC to the FCC-ee”, *JHEP* **09** (2024) 091, [doi:10.1007/JHEP09\(2024\)091](https://doi.org/10.1007/JHEP09(2024)091), [arXiv:2404.12809](https://arxiv.org/abs/2404.12809).
- [6] J. de Blas et al., “Constraining new physics effective interactions via a global fit of electroweak, Drell–Yan, Higgs, top, and flavour observables”, 2025. [arXiv:2507.06191](https://arxiv.org/abs/2507.06191).
- [7] M. D. Schwartz, “Modern machine learning and particle physics”, *Harv. Data Sci. Rev.* **3** (2021) 2, [doi:10.1162/99608f92.beeb1183](https://doi.org/10.1162/99608f92.beeb1183), [arXiv:2103.12226](https://arxiv.org/abs/2103.12226).
- [8] P. Ferreira da Silva, “Physics of the top quark at the LHC: An appraisal and outlook of the road ahead”, *Ann. Rev. Nucl. Part. Sci.* **73** (2023) 255, [doi:10.1146/annurev-nucl-102419-052854](https://doi.org/10.1146/annurev-nucl-102419-052854).
- [9] CMS Collaboration, “Observation of a pseudoscalar excess at the top quark pair production threshold”, *Rep. Prog. Phys.* **88** (2025) 087801, [doi:10.1088/1361-6633/adf7d3](https://doi.org/10.1088/1361-6633/adf7d3), [arXiv:2503.22382](https://arxiv.org/abs/2503.22382).
- [10] CMS Collaboration, “Search for heavy pseudoscalar and scalar bosons decaying to a top quark pair in proton-proton collisions at $\sqrt{s} = 13$ TeV”, *Rep. Prog. Phys.* **88** (2025) 127801, [doi:10.1088/1361-6633/ae2207](https://doi.org/10.1088/1361-6633/ae2207), [arXiv:2507.05119](https://arxiv.org/abs/2507.05119).
- [11] ATLAS Collaboration, “Observation of a cross-section enhancement near the $t\bar{t}$ production threshold in $\sqrt{s} = 13$ TeV pp collisions with the ATLAS detector”, ATLAS Conference Note ATLAS-CONF-2025-008, 2025.
- [12] B. Fuks, K. Hagiwara, K. Ma, and Y.-J. Zheng, “Simulating toponium formation signals at the LHC”, *Eur. Phys. J. C* **85** (2025) 157, [doi:10.1140/epjc/s10052-025-13853-3](https://doi.org/10.1140/epjc/s10052-025-13853-3), [arXiv:2411.18962](https://arxiv.org/abs/2411.18962).
- [13] M. V. Garzelli et al., “Updated predictions for toponium production at the LHC”, *Phys. Lett. B* **866** (2025) 139532, [doi:10.1016/j.physletb.2025.139532](https://doi.org/10.1016/j.physletb.2025.139532), [arXiv:2412.16685](https://arxiv.org/abs/2412.16685).
- [14] F. Maltoni, C. Severi, S. Tentori, and E. Vryonidou, “Quantum detection of new physics in top-quark pair production at the LHC”, *JHEP* **03** (2024) 099, [doi:10.1007/JHEP03\(2024\)099](https://doi.org/10.1007/JHEP03(2024)099), [arXiv:2401.08751](https://arxiv.org/abs/2401.08751).
- [15] H. Bahl, R. Kumar, and G. Weiglein, “Impact of interference effects on Higgs-boson searches in the di-top final state at the LHC”, *JHEP* **05** (2025) 098, [doi:10.1007/JHEP05\(2025\)098](https://doi.org/10.1007/JHEP05(2025)098), [arXiv:2503.02705](https://arxiv.org/abs/2503.02705).

[16] P. Nason, E. Re, and L. Rottoli, “Spin correlations in $t\bar{t}$ production and decay at the LHC in QCD perturbation theory”, *JHEP* **10** (2025) 149, [doi:10.1007/JHEP10\(2025\)149](https://doi.org/10.1007/JHEP10(2025)149), [arXiv:2505.00096](https://arxiv.org/abs/2505.00096).

[17] Y. Matsuoka, “Possible mixing between elementary and bound state fields in the $t\bar{t}$ production excess at the LHC”, 2025. [arXiv:2510.16828](https://arxiv.org/abs/2510.16828).

[18] B. Fuks, A. Hossain, and J. Keaveney, “Statistical indications of toponium formation in top quark pair production”, 2025. [arXiv:2511.02040](https://arxiv.org/abs/2511.02040).

[19] T. Flacke et al., “New physics in toponium’s shadow?”, 2025. [arXiv:2512.03220](https://arxiv.org/abs/2512.03220).

[20] G. Arcadi and A. Djouadi, “Interpreting the current Higgs excesses at the LHC in the 2HD+a framework”, 2025. [arXiv:2512.08807](https://arxiv.org/abs/2512.08807).

[21] ATLAS Collaboration, “The quest to discover supersymmetry at the ATLAS experiment”, *Phys. Rept.* **1116** (2025) 261, [doi:10.1016/j.physrep.2024.09.010](https://doi.org/10.1016/j.physrep.2024.09.010), [arXiv:2403.02455](https://arxiv.org/abs/2403.02455).

[22] ATLAS Collaboration, “Exploration at the high-energy frontier: ATLAS Run 2 searches investigating the exotic jungle beyond the standard model”, *Phys. Rept.* **1116** (2025) 301, [doi:10.1016/j.physrep.2024.10.001](https://doi.org/10.1016/j.physrep.2024.10.001), [arXiv:2403.09292](https://arxiv.org/abs/2403.09292).

[23] CMS Collaboration, “Searches for Higgs boson production through decays of heavy resonances”, *Phys. Rept.* **1115** (2025) 368, [doi:10.1016/j.physrep.2024.09.004](https://doi.org/10.1016/j.physrep.2024.09.004), [arXiv:2403.16926](https://arxiv.org/abs/2403.16926).

[24] ATLAS Collaboration, “Characterising the Higgs boson with ATLAS data from the LHC Run 2”, *Phys. Rept.* **1116** (2025) 4, [doi:10.1016/j.physrep.2024.11.001](https://doi.org/10.1016/j.physrep.2024.11.001), [arXiv:2404.05498](https://arxiv.org/abs/2404.05498).

[25] ATLAS Collaboration, “Electroweak, QCD and flavour physics studies with ATLAS data from Run 2 of the LHC”, *Phys. Rept.* **1116** (2025) 57, [doi:10.1016/j.physrep.2024.12.003](https://doi.org/10.1016/j.physrep.2024.12.003), [arXiv:2404.06829](https://arxiv.org/abs/2404.06829).

[26] ATLAS Collaboration, “Climbing to the top of the ATLAS 13 TeV data”, *Phys. Rept.* **1116** (2025) 127, [doi:10.1016/j.physrep.2024.12.004](https://doi.org/10.1016/j.physrep.2024.12.004), [arXiv:2404.10674](https://arxiv.org/abs/2404.10674).

[27] ATLAS Collaboration, “ATLAS searches for additional scalars and exotic Higgs boson decays with the LHC Run 2 dataset”, *Phys. Rept.* **1116** (2025) 184, [doi:10.1016/j.physrep.2024.09.002](https://doi.org/10.1016/j.physrep.2024.09.002), [arXiv:2405.04914](https://arxiv.org/abs/2405.04914).

[28] CMS Collaboration, “Overview of high-density QCD studies with the CMS experiment at the LHC”, *Phys. Rept.* **1115** (2025) 219, [doi:10.1016/j.physrep.2024.11.007](https://doi.org/10.1016/j.physrep.2024.11.007), [arXiv:2405.10785](https://arxiv.org/abs/2405.10785).

[29] CMS Collaboration, “Dark sector searches with the CMS experiment”, *Phys. Rept.* **1115** (2025) 448, [doi:10.1016/j.physrep.2024.09.013](https://doi.org/10.1016/j.physrep.2024.09.013), [arXiv:2405.13778](https://arxiv.org/abs/2405.13778).

[30] CMS Collaboration, “Review of searches for vector-like quarks, vector-like leptons, and heavy neutral leptons in proton-proton collisions at $\sqrt{s} = 13$ TeV at the CMS experiment”, *Phys. Rept.* **1115** (2025) 570, [doi:10.1016/j.physrep.2024.09.012](https://doi.org/10.1016/j.physrep.2024.09.012), [arXiv:2405.17605](https://arxiv.org/abs/2405.17605).

[31] CMS Collaboration, “Stairway to discovery: A report on the CMS programme of cross section measurements from millibarns to femtobarns”, *Phys. Rept.* **1115** (2025) 3, [doi:10.1016/j.physrep.2024.11.005](https://doi.org/10.1016/j.physrep.2024.11.005), [arXiv:2405.18661](https://arxiv.org/abs/2405.18661).

[32] R. M. Neal, “Computing likelihood functions for high-energy physics experiments when distributions are defined by simulators with nuisance parameters”, in *Proc. LHC Workshop*

on Statistical Issues for LHC Physics (PHYSTAT-LHC): Geneva, Switzerland, June 27–29, 2007, p. 111. 2007. [doi:10.5170/CERN-2008-001.111](https://doi.org/10.5170/CERN-2008-001.111).

- [33] K. Cranmer, J. Pavez, and G. Louppe, “Approximating likelihood ratios with calibrated discriminative classifiers”, 2015. [arXiv:1506.02169](https://arxiv.org/abs/1506.02169).
- [34] P. De Castro and T. Dorigo, “INFERNO: Inference-aware neural optimisation”, *Comput. Phys. Commun.* **244** (2019) 170, [doi:10.1016/j.cpc.2019.06.007](https://doi.org/10.1016/j.cpc.2019.06.007), [arXiv:1806.04743](https://arxiv.org/abs/1806.04743).
- [35] S. Wunsch, S. Jörger, R. Wolf, and G. Quast, “Optimal statistical inference in the presence of systematic uncertainties using neural network optimization based on binned Poisson likelihoods with nuisance parameters”, *Comput. Softw. Big Sci.* **5** (2021) 4, [doi:10.1007/s41781-020-00049-5](https://doi.org/10.1007/s41781-020-00049-5), [arXiv:2003.07186](https://arxiv.org/abs/2003.07186).
- [36] N. Simpson and L. Heinrich, “NEOS: End-to-end-optimised summary statistics for high energy physics”, in *Proc. 20th International Workshop on Advanced Computing and Analysis Techniques in Physics Research (ACAT 2021): Daejeon, South Korea, November 29–December 03, 2021*. 2023. [arXiv:2203.05570](https://arxiv.org/abs/2203.05570). [J. Phys. Conf. Ser. 2438 (2023) 012105]. [doi:10.1088/1742-6596/2438/1/012105](https://doi.org/10.1088/1742-6596/2438/1/012105).
- [37] CMS Collaboration, “Development of systematic uncertainty-aware neural network trainings for binned-likelihood analyses at the LHC”, *Eur. Phys. J. C* **85** (2025) 1360, [doi:10.1140/epjc/s10052-025-14713-w](https://doi.org/10.1140/epjc/s10052-025-14713-w), [arXiv:2502.13047](https://arxiv.org/abs/2502.13047).
- [38] G. Cowan, “A survey of unfolding methods for particle physics”, in *Proc. Conference on Advanced Statistical Techniques in Particle Physics: Durham, UK, March 18–22, 2002*. 2002. [Conf. Proc. C 0203181 (2002) 248].
- [39] R. A. Fisher, “On the mathematical foundations of theoretical statistics”, *Phil. Trans. Roy. Soc. Lond. A* **222** (1922) 309, [doi:10.1098/rsta.1922.0009](https://doi.org/10.1098/rsta.1922.0009).
- [40] G. Cowan, K. Cranmer, E. Gross, and O. Vitells, “Asymptotic formulae for likelihood-based tests of new physics”, *Eur. Phys. J. C* **71** (2011) 1554, [doi:10.1140/epjc/s10052-011-1554-0](https://doi.org/10.1140/epjc/s10052-011-1554-0), [arXiv:1007.1727](https://arxiv.org/abs/1007.1727). [Erratum: [doi:10.1140/epjc/s10052-013-2501-z](https://doi.org/10.1140/epjc/s10052-013-2501-z)].
- [41] ATLAS and CMS Collaborations, and LHC Higgs Combination Group, “Procedure for the LHC Higgs boson search combination in Summer 2011”, Technical Report CMS-NOTE-2011-005, ATL-PHYS-PUB-2011-11, 2011.
- [42] CMS Collaboration, “The CMS statistical analysis and combination tool: COMBINE”, *Comput. Softw. Big Sci.* **8** (2024) 19, [doi:10.1007/s41781-024-00121-4](https://doi.org/10.1007/s41781-024-00121-4), [arXiv:2404.06614](https://arxiv.org/abs/2404.06614).
- [43] J. Alwall et al., “The automated computation of tree-level and next-to-leading order differential cross sections, and their matching to parton shower simulations”, *JHEP* **07** (2014) 079, [doi:10.1007/JHEP07\(2014\)079](https://doi.org/10.1007/JHEP07(2014)079), [arXiv:1405.0301](https://arxiv.org/abs/1405.0301).
- [44] NNPDF Collaboration, “Parton distributions from high-precision collider data”, *Eur. Phys. J. C* **77** (2017) 663, [doi:10.1140/epjc/s10052-017-5199-5](https://doi.org/10.1140/epjc/s10052-017-5199-5), [arXiv:1706.00428](https://arxiv.org/abs/1706.00428).
- [45] C. Bierlich et al., “A comprehensive guide to the physics and usage of PYTHIA 8.3”, *SciPost Phys. Codeb.* **8** (2022) [doi:10.21468/SciPostPhysCodeb.8](https://doi.org/10.21468/SciPostPhysCodeb.8), [arXiv:2203.11601](https://arxiv.org/abs/2203.11601).
- [46] DELPHES 3 Collaboration, “DELPHES 3: a modular framework for fast simulation of a generic collider experiment”, *JHEP* **02** (2014) 057, [doi:10.1007/JHEP02\(2014\)057](https://doi.org/10.1007/JHEP02(2014)057), [arXiv:1307.6346](https://arxiv.org/abs/1307.6346).

[47] M. Selvaggi, “DELPHEs 3: A modular framework for fast-simulation of generic collider experiments”, in *Proc. 15th International Workshop on Advanced Computing and Analysis Techniques in Physics Research (ACAT 2013): Beijing, China, May 16–21, 2013*. 2014. [J. Phys. Conf. Ser. 523 (2014) 012033]. [doi:10.1088/1742-6596/523/1/012033](https://doi.org/10.1088/1742-6596/523/1/012033).

[48] A. Mertens, “New features in DELPHES 3”, in *Proc. 16th International Workshop on Advanced Computing and Analysis Techniques in Physics Research (ACAT 2014): Prague, Czechia, September 1–5, 2014*. 2015. [J. Phys. Conf. Ser. 608 (2015) 012045]. [doi:10.1088/1742-6596/608/1/012045](https://doi.org/10.1088/1742-6596/608/1/012045).

[49] P. Artoisenet, R. Frederix, O. Mattelaer, and R. Rietkerk, “Automatic spin-entangled decays of heavy resonances in Monte Carlo simulations”, *JHEP* **03** (2013) 015, [doi:10.1007/JHEP03\(2013\)015](https://doi.org/10.1007/JHEP03(2013)015), [arXiv:1212.3460](https://arxiv.org/abs/1212.3460).

[50] M. Czakon and A. Mitov, “TOP++: a program for the calculation of the top-pair cross-section at hadron colliders”, *Comput. Phys. Commun.* **185** (2014) 2930, [doi:10.1016/j.cpc.2014.06.021](https://doi.org/10.1016/j.cpc.2014.06.021), [arXiv:1112.5675](https://arxiv.org/abs/1112.5675).

[51] B. Fuks, K. Hagiwara, K. Ma, and Y.-J. Zheng, “Signatures of toponium formation in LHC Run 2 data”, *Phys. Rev. D* **104** (2021) 034023, [doi:10.1103/PhysRevD.104.034023](https://doi.org/10.1103/PhysRevD.104.034023), [arXiv:2102.11281](https://arxiv.org/abs/2102.11281).

[52] V. S. Fadin, V. A. Khoze, and T. Sjöstrand, “On the threshold behaviour of heavy top production”, *Z. Phys. C* **48** (1990) 613, [doi:10.1007/BF01614696](https://doi.org/10.1007/BF01614696).

[53] Y. Sumino and H. Yokoya, “Bound-state effects on kinematical distributions of top quarks at hadron colliders”, *JHEP* **09** (2010) 034, [doi:10.1007/JHEP09\(2010\)034](https://doi.org/10.1007/JHEP09(2010)034), [arXiv:1007.0075](https://arxiv.org/abs/1007.0075). [Erratum: [doi:10.1007/JHEP06\(2016\)037](https://doi.org/10.1007/JHEP06(2016)037)].

[54] A. Paszke et al., “PYTORCH: An imperative style, high-performance deep learning library”, in *Proc. 33rd Conference on Neural Information Processing Systems (NeurIPS 2019): Vancouver, Canada, December 08–14, 2019*. 2019. [arXiv:1912.01703](https://arxiv.org/abs/1912.01703).

[55] V. Nair and G. E. Hinton, “Rectified linear units improve restricted Boltzmann machines”, in *Proc. 27th International Conference on Machine Learning (ICML 2010): Haifa, Israel, June 21–24, 2010*, p. 807. 2010.

[56] CMS Collaboration, “Measurement of the differential cross section for top quark pair production in pp collisions at $\sqrt{s} = 8$ TeV”, *Eur. Phys. J. C* **75** (2015) 542, [doi:10.1140/epjc/s10052-015-3709-x](https://doi.org/10.1140/epjc/s10052-015-3709-x), [arXiv:1505.04480](https://arxiv.org/abs/1505.04480).

[57] CMS Collaboration, “Measurement of $t\bar{t}$ normalised multi-differential cross sections in pp collisions at $\sqrt{s} = 13$ TeV, and simultaneous determination of the strong coupling strength, top quark pole mass, and parton distribution functions”, *Eur. Phys. J. C* **80** (2020) 658, [doi:10.1140/epjc/s10052-020-7917-7](https://doi.org/10.1140/epjc/s10052-020-7917-7), [arXiv:1904.05237](https://arxiv.org/abs/1904.05237).

[58] ALICE Collaboration, “Transverse sphericity of primary charged particles in minimum bias proton-proton collisions at $\sqrt{s} = 0.9, 2.76$ and 7 TeV”, *Eur. Phys. J. C* **72** (2012) 2124, [doi:10.1140/epjc/s10052-012-2124-9](https://doi.org/10.1140/epjc/s10052-012-2124-9), [arXiv:1205.3963](https://arxiv.org/abs/1205.3963).

[59] CMS Collaboration, “Jet energy scale and resolution in the CMS experiment in pp collisions at 8 TeV”, *JINST* **12** (2017) P02014, [doi:10.1088/1748-0221/12/02/P02014](https://doi.org/10.1088/1748-0221/12/02/P02014), [arXiv:1607.03663](https://arxiv.org/abs/1607.03663).

[60] ATLAS Collaboration, “Jet energy scale and resolution measured in proton-proton collisions

at $\sqrt{s} = 13$ TeV with the ATLAS detector”, *Eur. Phys. J. C* **81** (2021) 689, [doi:10.1140/epjc/s10052-021-09402-3](https://doi.org/10.1140/epjc/s10052-021-09402-3), [arXiv:2007.02645](https://arxiv.org/abs/2007.02645).

- [61] I. J. Good, “Rational decisions”, *J. Royal Stat. Soc. B* **14** (1952) 107, [doi:10.1111/j.2517-6161.1952.tb00104.x](https://doi.org/10.1111/j.2517-6161.1952.tb00104.x).
- [62] S. Wunsch, R. Friese, R. Wolf, and G. Quast, “Identifying the relevant dependencies of the neural network response on characteristics of the input space”, *Comput. Softw. Big Sci.* **2** (2018) 5, [doi:10.1007/s41781-018-0012-1](https://doi.org/10.1007/s41781-018-0012-1), [arXiv:1803.08782](https://arxiv.org/abs/1803.08782).
- [63] A. Butter, T. Plehn, N. Soybelman, and J. Brehmer, “Back to the formula—LHC edition”, *SciPost Phys.* **16** (2024) 037, [doi:10.21468/SciPostPhys.16.1.037](https://doi.org/10.21468/SciPostPhys.16.1.037), [arXiv:2109.10414](https://arxiv.org/abs/2109.10414).
- [64] S. AbdusSalam, S. Abel, and M. Crispim Romão, “Symbolic regression for beyond the standard model physics”, *Phys. Rev. D* **111** (2025) 015022, [doi:10.1103/PhysRevD.111.015022](https://doi.org/10.1103/PhysRevD.111.015022), [arXiv:2405.18471](https://arxiv.org/abs/2405.18471).
- [65] Z. Dong, K. Kong, K. T. Matchev, and K. Matcheva, “Is the machine smarter than the theorist: Deriving formulas for particle kinematics with symbolic regression”, *Phys. Rev. D* **107** (2023) 055018, [doi:10.1103/PhysRevD.107.055018](https://doi.org/10.1103/PhysRevD.107.055018), [arXiv:2211.08420](https://arxiv.org/abs/2211.08420).